Boundary-Layer Calculations in the Inverse Mode for Incompressible Flows over Infinite Swept Wings

S. F. Radwan* and S. G. Lekoudis†
Georgia Institute of Technology, Atlanta, Georgia

The boundary-layer equations for incompressible steady turbulent flow are solved in the inverse mode under the infinite swept cylinder assumption. The Keller box is used with weighted upwinding in order to suppress oscillations in the solution. An anisotropic eddy-viscosity formula is used for modeling the turbulence. The computed results are compared with measured data. The scheme allows marching into the region of three-dimensional separated flow. Good agreement with experiments was obtained.

I. Introduction

THE computation of three-dimensional separated flows is of interest in several areas of applied aerodynamics. Three-dimensional separated flows occur on the unswept afterbodies of military transports, in regions of shock/boundary-layer interactions, or on the upper surface of wings. These few flowfields are only part of a large number of flowfields around vehicles, where three-dimensional separated flows are present.

An arbitrary classification of ways of computing three-dimensional viscous flowfields follows. One category consists of the methods that solve the three-dimensional Navier-Stokes equations for the whole field. In favor of this category is the increasing memory and speed of the available computers and, usually, the simplicity of coding as compared with the second category. The second category consists of methods that use different approximations to the Navier-Stokes equations for different parts of the flowfield and then combine the solutions. In its favor is the increased resolution available because of the segmentation of the flowfield, and, sometimes, the faster convergence in terms of total execution time. Moreover, related to the problem of the resolution is the decreased amount of numerical diffusion present, which increases the usefulness of the final answer. In spite of the advantages, the vast majority of the calculations that belong to the second category are done for attached three-dimensional flows.

If one attempts to use the second approach for computing three-dimensional separated flows, he has to decide on the equations that he will use in the area where the separation region originates on the body. This question, of what equations to use, has been asked many times before, and it is related to the singularity of the boundary-layer equations when the pressure is prescribed. The appearance of the singularity does not necessarily mean that the validity of the boundary-layer assumptions is lost. However, it can be interpreted as an indication of separation. This is not always justifiable. An illuminating discussion about the subject is in the introduction of Ref. 1. The singularity is avoided when the boundary-layer equations are solved in the inverse mode.

Inverse boundary-layer calculations for two-dimensional flows have been reported several times before in the literature. References 2-9 describe different methods that allow one to march into the separated region using prescribed displacement thickness or skin friction distributions. Also viscid/inviscid coupling procedures have been developed that include regions of separated flow. Such procedures are reported in Refs. 10-17, and the capability of the schemes to numerically capture separated flow regions is demonstrated. Reference 18 includes a favorable comparison between full Navier-Stokes calculations and inverse boundary-layer calculations. In spite of the number of works performed for the two-dimensional case, it seems that the range of validity of the boundary-layer calculations in the inverse mode is still judged by its convergence. Moreover, the experience in the use of the inverse boundary-layer calculations for three-dimensional separated flow is very limited.

In Ref. 1 an integral method was used to solve the boundary-layer equations. Some of the relative advantages and disadvantages of integral techniques vs finite difference techniques for solving the boundary-layer equations are as follows. The integral methods are faster and usually require less computer memory. Because a shape is assumed for the velocity profiles, it is difficult to examine relatively sophisticated turbulence models. Moreover, higher-order effects such as the variation of the pressure in the direction normal to the wall or the effects of curvature are difficult to incorporate. These effects seem to be important in regions close to separation as shown from measurements in both two- and three-dimensional flows.[19,20]

In this work, the three-dimensional boundary-layer equations for laminar and turbulent flow are solved in the inverse mode under the ideal and approximate infinite yawed cylinder assumptions. The Keller box is used with a modification that suppresses oscillations in the solution. The calculations are compared with the measurements reported in Ref. 1, and the capability of the scheme to march into the separated flow region is demonstrated. After this work was completed, the authors found conclusions similar to those reported here in Refs. 25-27.

The analytical formulation and the turbulence model are described in Sec. II, the numerical procedure in Sec. III, and the results in Sec. IV.

II. The Analytical Formulation

Governing Equations and the Boundary Conditions

The equations for three-dimensional boundary layers in steady, incompressible, turbulent flow over an infinite yawed cylinder, whose generator is parallel to the z axis of an x, y, z

Presented as Paper 83-0454 at the AIAA 21st Aerospace Sciences Meeting, Reno, Nev., Jan. 10-13, 1983; submitted Feb. 25, 1983; revision received Sept. 1, 1983. Copyright © American Institute of Aeronautics and Astronautics, Inc., 1983. All rights reserved.

*Graduate Research Assistant, School of Aerospace Engineering. Student Member AIAA.

†Associate Professor, School of Aerospace Engineering. Member AIAA.

Cartesian coordinate system, shown in Fig. 1, are:

$$\frac{\partial \bar{u}^*}{\partial x^*} + \frac{\partial \bar{v}^*}{\partial y^*} = 0 \tag{1a}$$

$$\bar{u}^* \frac{\partial \bar{u}^*}{\partial x^*} + v^* \frac{\partial \bar{u}^*}{\partial y^*} = -\frac{1}{\rho} \frac{\partial \bar{p}^*}{\partial x^*} + \frac{\partial}{\partial y^*} \left(\nu^* \frac{\partial \bar{u}^*}{\partial y^*} - \overline{u^{*\prime} v^{*\prime}} \right) \tag{1b}$$

$$\bar{u}^* \frac{\partial \bar{w}^*}{\partial x^*} + \bar{v}^* \frac{\partial \bar{w}^*}{\partial y^*} = -\frac{1}{\rho^*} \frac{\partial p^*}{\partial z^*} + \frac{\partial}{\partial y^*} + \frac{\partial}{\partial y^*} \left(\nu^* \frac{\partial \bar{w}^*}{\partial y^*} - \overline{w^{*\prime} v^{*\prime}} \right) \tag{1c}$$

In Eqs. (1) stars denote dimensional quantities; bars denote time averages; primes denote fluctuating quantities; u, v, w are the velocity components in the x, y, z directions, respectively; ρ is the density; p the pressure, and ν the kinematic viscosity. Note that the term $-1/\rho(\partial p/\partial z)$ is retained in order to apply the infinite yawed cylinder conditions both in an ideal and approximate way.

We introduce an algebraic eddy-viscosity for the Reynolds stresses,[21]

$$-\overline{u^{*\prime} v^{*\prime}} = \nu^* \left[(b_1 - 1) \frac{\partial \bar{u}^*}{\partial y^*} + b_2 \frac{\partial w^*}{\partial y^*} \right] \tag{2a}$$

$$-\overline{w^{*\prime} v^{*\prime}} = \nu^* \left[b_2 \frac{\partial \bar{w}^*}{\partial y^*} + (b_3 - 1) \frac{\partial \bar{u}^*}{\partial y^*} \right] \tag{2b}$$

When the equations are solved in the inverse mode we introduce the two-component vector potential,

$$\psi^* = \sqrt{U_\infty^* \nu^* L^*} f(x, \eta) \tag{3a}$$

$$\phi^* = \sqrt{U_\infty^* \nu^* L^*} g(x, \eta) \tag{3b}$$

so that,

$$\bar{u}^* = \frac{\partial \psi^*}{\partial y^*} \tag{4a}$$

$$\bar{w}^* = \frac{\partial \phi^*}{\partial y^*} \tag{4b}$$

$$\bar{v}^* = -\left(\frac{\partial \psi^*}{\partial x^*} + \frac{\partial \phi^*}{\partial z^*} \right) \tag{4c}$$

and the boundary-layer coordinates,

$$x = \frac{x^*}{L^*} \tag{5a}$$

$$\eta = \frac{y^*}{L^*} \sqrt{R_L} \tag{5b}$$

$$R_L = \frac{U_\infty^* L^*}{\nu^*} \tag{5c}$$

with U and L being the reference velocity and length.

Then the thin shear layer equations become

$$(b_1 f'')' + \bar{U}_e \frac{d\bar{U}_e}{dx} = f' \frac{\partial f'}{\partial x} - f'' \frac{\partial f}{\partial x} - (b_2 g'')' \tag{6a}$$

$$(b_3 g'')' + \bar{U}_e \frac{d\bar{w}_e}{dx} = f' \frac{\partial g'}{\partial x} - g'' \frac{\partial f}{\partial x} - (b_2 f'')' \tag{6b}$$

In Eqs. (6) primes denote derivatives with respect to η. The second term in Eq. (6b) is retained as an approximation to the nonzero $-1/\rho(\partial p/\partial z)$ term. This is possible by observing that the Euler equations at the boundary-layer edge give

$$\bar{u}_e^* \frac{\partial \bar{u}_e^*}{\partial x^*} + \bar{w}_e^* \frac{\partial \bar{u}_e^*}{\partial z^*} = -\frac{1}{\rho^*} \frac{\partial \bar{p}^*}{\partial x^*} \tag{7a}$$

$$\bar{u}_e^* \frac{\partial \bar{w}_e^*}{\partial x^*} + \bar{w}_e^* \frac{\partial \bar{w}_e^*}{\partial z^*} = -\frac{1}{\rho^*} \frac{\partial \bar{p}^*}{\partial z^*} \tag{7b}$$

Equation (7b), without the second term of the left-hand side, is used to approximate a spanwise pressure gradient. This pressure gradient can be neglected in the calculations by using a flag in the input data.

The boundary conditions force the velocity to vanish at the wall which gives

$$f = f' = g = g' = 0 \text{ at } \eta = 0 \tag{8a}$$

The displacement thicknesses

$$\delta_x^* = \int_0^\infty \left(1 - \frac{\bar{u}^*}{u_e^*} \right) dy^* \tag{8b}$$

$$\delta_z^* = \int_0^\infty \left(1 - \frac{\bar{w}^*}{w_e^*} \right) dy^* \tag{8c}$$

are prescribed functions of x^*. The six conditions [Eqs. (8)] are used as boundary conditions in order to solve the system of Eqs. (6) numerically. Equations (8b) and (8c) are rewritten in terms of the two-component vector potential and are used as Dirichlet boundary conditions at the edge of the boundary layer.

The initial conditions for the inverse calculations can be generated in several ways. The experimental velocity profiles can be used, or velocity profiles formed by polynomial expressions, or solutions of the boundary-layer equations in the direct mode can also be used. The last procedure was followed in this work. Therefore, the equations were also solved in the direct mode. The two-component vector potential used in this case is

$$\psi^* = \sqrt{u_e^{**} x^*} f(x, \eta) \tag{9a}$$

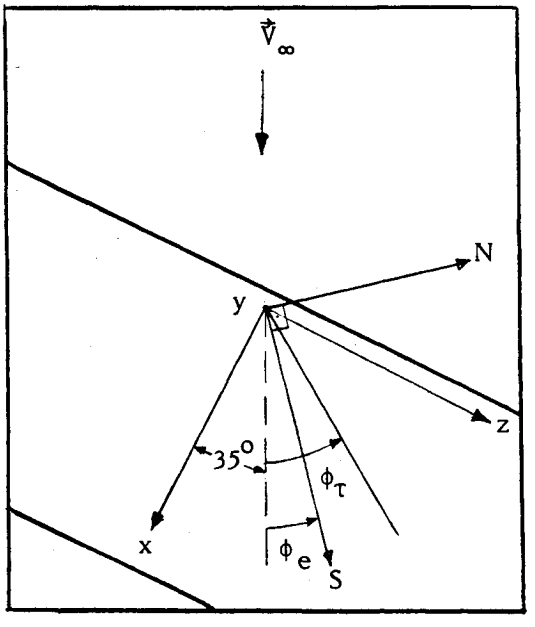

Fig. 1 Coordinate system.

$$\phi^* = \sqrt{\overline{u_e^*} \nu^* x^*} g(x,\eta) \overline{w_e^*/u_e^*} \tag{9b}$$

The velocities are still given by Eqs. (4) but the boundary-layer coordinates are

$$x = x^*/L^* \tag{10a}$$

$$\eta = \frac{y^*}{x^*}\sqrt{R_x} \tag{10b}$$

$$R_x = \overline{u_e^*} x/\nu^* \tag{10c}$$

Then the thin shear layer equations (1) become

$$(b_1 f'')' + \tfrac{1}{2}(1+p_2) f'' f + p_2 (1 - f'^2)$$

$$= x\left(f' \frac{\partial f'}{\partial x} - f'' \frac{\partial f}{\partial x}\right) - (b_2 g'')' \overline{w_e^*/u_e^*} \tag{11a}$$

$$(b_3 g'')' + \tfrac{1}{2}(1+p_2) f g'' + p_3 (1 - g' f')$$

$$= x\left(f' \frac{\partial g'}{\partial x} - g'' \frac{\partial f}{\partial x}\right) - (b_2 f'')' \overline{u_e^*/w_e^*} \tag{11b}$$

where

$$p_2 = \frac{x^*}{\overline{u_e^*}} \frac{\mathrm{d}\overline{u_e^*}}{\mathrm{d}x^*} \tag{12a}$$

$$p_3 = \frac{x^*}{\overline{w_e^*}} \frac{\mathrm{d}\overline{w_e^*}}{\mathrm{d}x^*} \tag{12b}$$

The boundary conditions for system (11) are:

$$f = f' = g = g' = 0 \text{ at } \eta = 0 \tag{13a}$$

$$f' = g' = 1 \qquad \text{at } \eta = \eta_e \tag{13b}$$

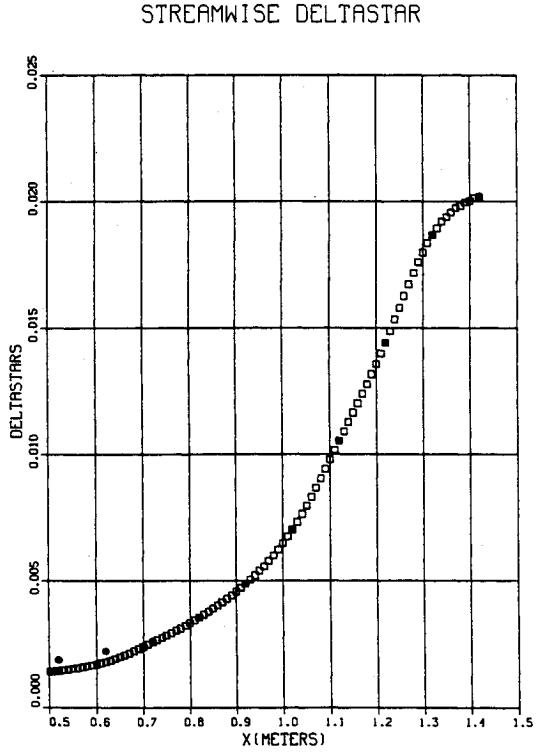

Fig. 2 Displacement thickness used in the calculation with the inverse mode.

Turbulence Model

The anisotropic eddy-viscosity model suggested by Rotta[21] is used. It is an algebraic eddy-viscosity model with

$$\epsilon_i^* = L^{*2}\left[\left(\frac{\partial u^*}{\partial y^*}\right)^2 + \left(\frac{\partial w^*}{\partial y^*}\right)^2 + (T-1)\frac{\left(\overline{w^*}\dfrac{\partial \overline{u^*}}{\partial y^*} - \overline{u^*}\dfrac{\partial \overline{w^*}}{\partial y^*}\right)^2}{(\overline{u^{*2}} + \overline{w^{*2}})}\right] \tag{14a}$$

$$\epsilon_o^* = 0.0168\left|\int_0^\infty [(\overline{u_e^{*2}} + \overline{w_e^{*2}})^{1/2} - (\overline{u^{*2}} + \overline{w^{*2}})^{1/2}]\mathrm{d}y^*\right| \tag{14b}$$

$$b_1 = \frac{\epsilon^*}{\nu^*}(\overline{u^{*2}} + T\overline{w^{*2}})/(\overline{u^{*2}} + \overline{w^{*2}}) \tag{14c}$$

$$b_2 = \frac{\epsilon^*}{\nu^*}(1-T)\overline{u^* w^*}/(\overline{u^{*2}} + \overline{w^{*2}}) \tag{14d}$$

$$b_3 = \frac{\epsilon^*}{\nu^*}(\overline{w^{*2}} + T\overline{u^{*2}})/(\overline{u^{*2}} + \overline{w^{*2}}) \tag{14e}$$

where ϵ^* is the turbulent viscosity and subscripts i and o indicate inner and outer regions. They are determined numerically so that at their common boundary $\epsilon_i = \epsilon_o$. The mixing length L is defined using the Cebeci-Smith model.[22] The parameter T, controlled from the input, changes the amount of anisotropy in the inner part of the boundary layer.

III. The Numerical Procedure

A code that solves the incompressible two-dimensional turbulent boundary-layer equations in the inverse mode is available in Ref. 22. We run the code, with modifications, for several test cases. It was found that, sometimes, oscillatory skin friction coefficients resulted from the converged solution. The same type of oscillations occurred for the case of three-dimensional flow. In order to eliminate these oscillations we modified the numerical scheme. The effect of the truncation error was controlled by computing with several grids.

The following dependent variables are used:

$$f = F_1 \qquad g = F_2 \tag{15a}$$

$$f' = U_1 \qquad g' = U_2 \tag{15b}$$

$$f'' = V_1 \qquad g'' = V_2 \tag{15c}$$

$$f_e = W_1 \qquad g_e = W_2 \tag{15d}$$

The system of Eqs. (6) can be rewritten in the form

$$F_1' = U_1 \tag{16a}$$

$$U_1' = V_1 \tag{16b}$$

$$(b_1 V_1)' = -W_1 \frac{\partial W_1}{\partial x} + U_1 \frac{\partial U_1}{\partial x} - V_1 \frac{\partial F_1}{\partial x} - (b_2 V_2)' \tag{16c}$$

$$W_1' = p_1(\eta, x) \tag{16d}$$

$$F_2' = U_2 \tag{17a}$$

$$U_2' = V_2 \tag{17b}$$

$$(b_3 V_2)' = -W_1 \frac{\partial W_2}{\partial x} + U_1 \frac{\partial U_2}{\partial x} - V_2 \frac{\partial F_1}{\partial x} - (b_2 V_1)' \tag{17c}$$

$$W_2' = p_2(\eta, x) \tag{17d}$$

Table 1 Comparison of results from direct and inverse calculations for three-dimensional laminar flow ($Re = 1.257 \times 10^6$, sweep angle = 45 deg)

x	U_e/U_{ref} (Direct)	U_e/U_{ref} (Inverse)	$c_{f_x} \times 10^3$ (Direct)	$c_{f_x} \times 10^3$ (Inverse)
0.09	0.691	0.691	1.1022	1.1020
0.11	0.688	0.688	0.9628	0.9632
0.13	0.684	0.684	0.8435	0.8425
0.15	0.680	0.680	0.7560	0.7562
0.17	0.677	0.677	0.6774	0.6765
0.19	0.673	0.673	0.6138	0.6138
0.21	0.670	0.670	0.5551	0.5545
0.23	0.666	0.666	0.5045	0.5044
0.25	0.662	0.662	0.4568	0.4564
0.27	0.659	0.659	0.4139	0.4138
x	w_e/U_{ref} (Direct)	w_e/U_{ref} (Inverse)	$c_{f_z} \times 10^3$ (Direct)	$c_{f_z} \times 10^3$ (Inverse)
0.09	0.707	0.707	1.1757	1.1754
0.11	0.707	0.707	1.0571	1.0570
0.13	0.707	0.707	0.9609	0.9598
0.15	0.707	0.707	0.8889	0.8885
0.17	0.707	0.707	0.8266	0.8251
0.19	0.707	0.707	0.7761	0.7754
0.21	0.707	0.707	0.7307	0.7290
0.23	0.707	0.707	0.6919	0.6909
0.25	0.707	0.707	0.6560	0.6542
0.27	0.707	0.707	0.6242	0.6229

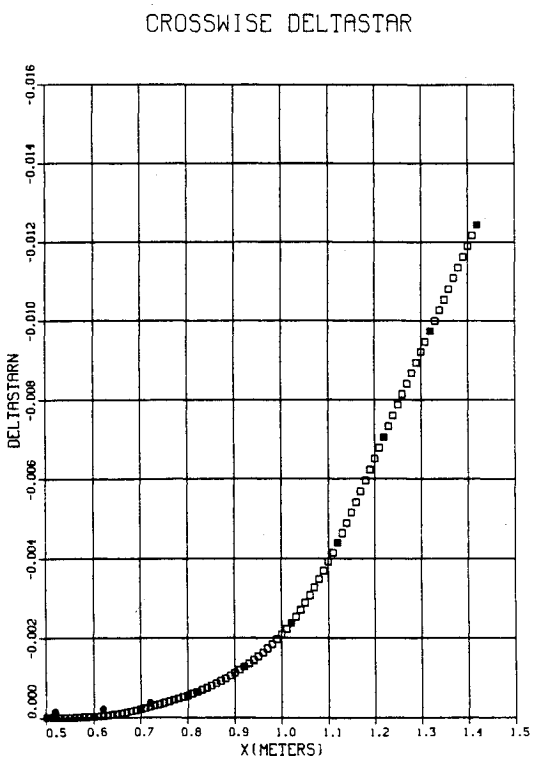

Fig. 3 Displacement thickness used in the calculation with the inverse mode.

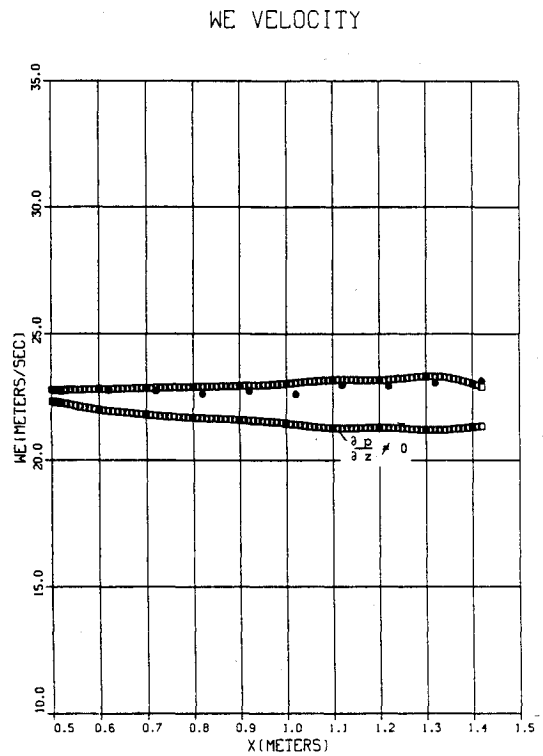

Fig. 4 Calculations in the inverse mode and comparison with experiments for the w_e velocity component.

The functions $p_1(\eta,x)$ and $p_2(\eta,x)$ can be prescribed from considerations of the variation of the pressure across the boundary layer. However in the results reported in this study, they are set equal to zero.

Equations (16) and (17) are coupled because b is a function U_1, V_1, U_2, and V_2. This happens even under the ideal swept cylinder assumption. Then the first term on the right-hand side of Eq. (17c) is identically zero. The equations are uncoupled only for the case of laminar flow. The system of Eqs. (17) is linear, provided the quantities with subscript *1*, and b's are known.

The solution procedure is based on Keller box scheme.[6,7,22] The system of Eqs. (16) is linearized and a Newton iteration is used together with an inversion of a block tridiagonal matrix. The element matrices are 4×4 square matrices. Then the system of Eqs. (17) is solved without any linearization since it is already linear for the quantities with subscript *2*. The same solver is used to invert the block tridiagonal matrix.

Note that the full three-dimensional problem involves two extra steps in the solution procedure. The first step is the inclusion of the extra terms on the right-hand side of Eqs. (16) and (17). The second step, which is optical, is the use of

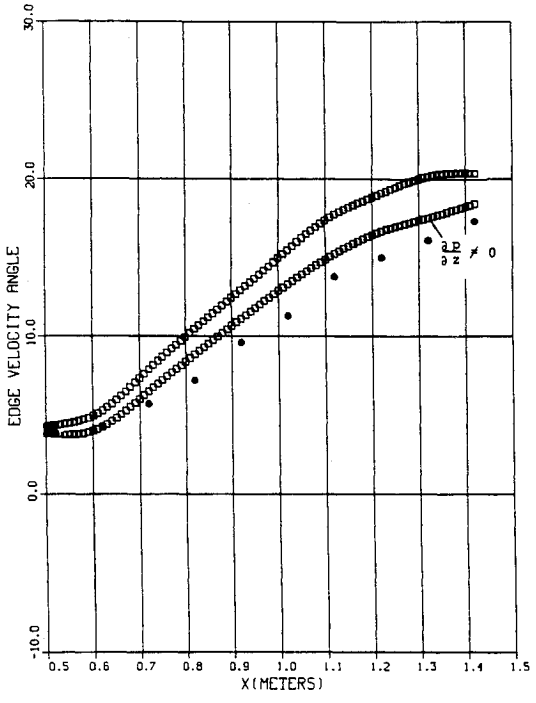

Fig. 5 Calculations in the inverse mode and comparison with experiments for the edge velocity direction.

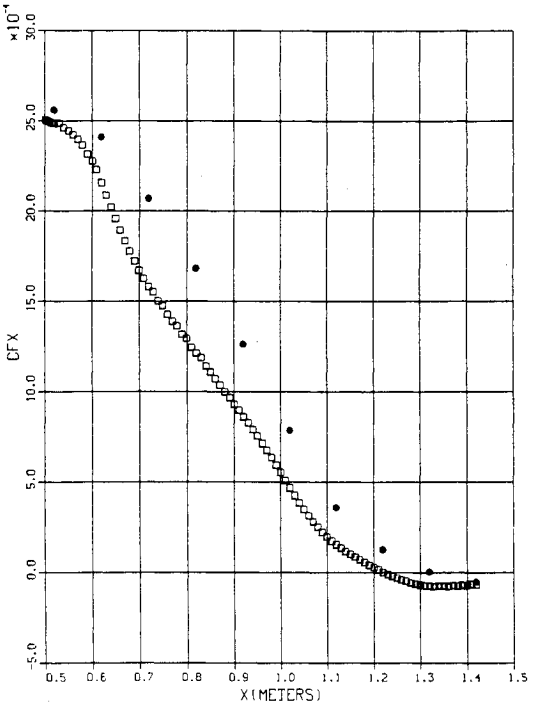

Fig. 6 Calculations in the inverse mode and comparison with experiments for the c_{f_x} distribution.

Newton's linearization in Eqs. (17). The solver remains identical. Such calculations will be reported in the future.

The variation of the box scheme that suppresses the oscillations in the skin friction coefficient works as follows. If we call B the station where the boundary-layer quantities are known, C the station before it, and A the station we are solving for, the Keller box centers using the midpoint between A and B. In the original scheme only quantities at A and B are used. In this scheme the quantities q at B are replaced by

$$q_B = rq_C + (1-r)q_B \tag{18}$$

where r is an upwinding parameter between zero and one. Equation (18) makes the scheme formally first-order accurate and a three-point scheme in the marching direction.

In the reversed flow region the Reyhner and Flugge-Lotz approximation is used in two ways. Either U_I is set equal to zero, or its negative is used, whenever U_I itself is negative. The results are practically insensitive to the choice made.

IV. Results and Discussion

We computed two-dimensional, separated, turbulent boundary-layer flows in order to compare with measured data. The computed and measured freestream velocity profiles and skin friction coefficients showed the same level of agreement that was shown in previous calculations. The measurements are from Ref. 19 and from the paper of Chu and Young.[16] The initial profiles are generated by computing in the direct mode and obtaining a velocity profile that has skin friction coefficient and displacement thickness close to the ones measured in the most upwind station. The measured displacement thicknesses are interpolated using a cubic spline. The calculations predict the separation and reproduce the measured freestream velocities and skin friction with reasonable accuracy.

In order to examine the validity of the calculations for the three-dimensional boundary-layer case, the displacement thicknesses computed in the direct mode were used as input for the calculations in the inverse mode. Table 1 shows the

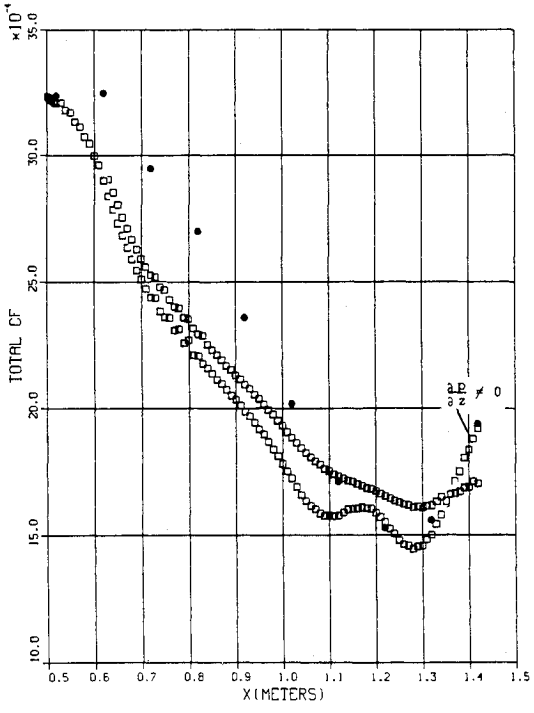

Fig. 7 Calculations in the inverse mode and comparison with experiments for the total c_f distribution.

comparison between the computed freestream velocities and skin friction coefficients for the case of laminar flow. Reasonable agreement is obtained.

The experience gained from these calculations suggests that the initial profile is very important. A small mismatch between the profile's displacement thickness and the measured displacement thickness downstream, results in severe oscillations in the solution. Therefore effort was devoted to obtain initial profiles for the data of Ref. 23. These data are for a separating turbulent boundary layer under conditions that correspond closely to the infinite swept wing conditions.

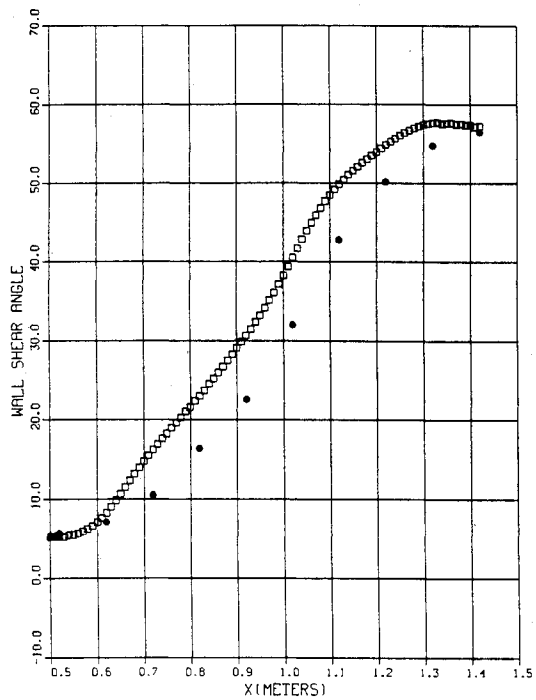

Fig. 8 Calculations in the inverse mode and comparison with experiments for the angle of the wall shear.

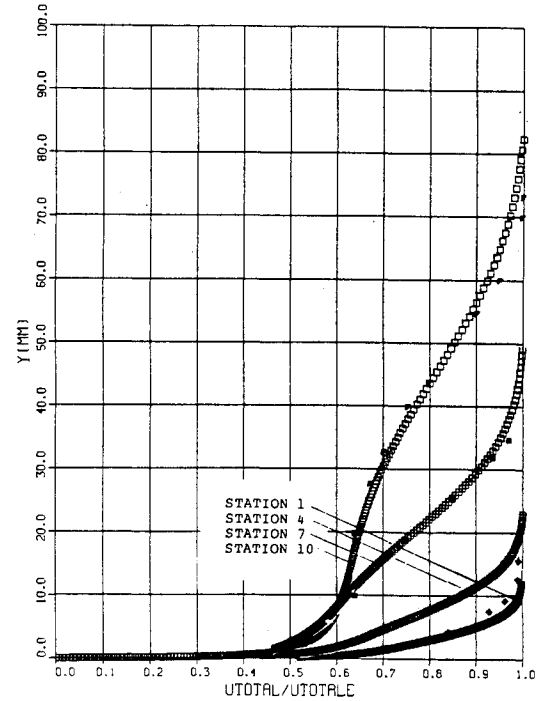

Fig. 10 Calculations in the inverse mode and comparison with experiments for the velocity magnitude.

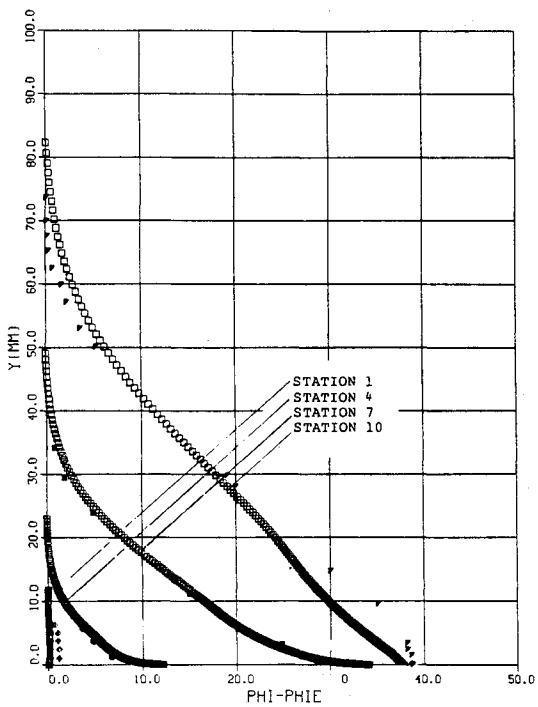

Fig. 9 Calculations in the inverse mode and comparison with experiments for the velocity direction.

The measured velocity distribution at the boundary-layer edge, with the anisotropy parameter T set equal to one, is used to compute in the direct mode. The computed quantities grossly misrepresent the development of the boundary layer. This is in agreement with previous calculations (Paper 16 of Ref. 24). However, at the beginning of the measuring stations, numbered 1 through 10 in Ref. 23, the computed boundary-layer properties agree with the measured properties reasonably well, except for the displacement thicknesses (as defined in Ref. 23).

Because of the discussed disagreement of the measured and computed displacement thicknesses at the beginning of the measuring stations, when the direct mode is used, the following procedure is followed. The displacement thicknesses used in the calculations with the inverse mode, shown in Figs. 2 and 3, are slightly different than the measured ones at the first two stations. As shown in Figs. 3-10 the initial boundary-layer properties agree reasonably well with the measurements. It is also shown in these figures that the computations reproduce the measured growth of the boundary layer, including the separation. The separation location was computed without any difficulty. The differences between certain computed quantities created by the $\partial p/\partial z$ term in the equations is confined to the skin friction and edge velocities in the z direction. In Figs. 9 and 10 it is shown that the calculations reliably reproduced the measured turbulent velocity profile *inside* the separated region. In the measurements[23] it is shown that station 10 is inside the separated region. The distances of the measurement stations 1, 4, 7, and 10 from the origin of the streamwise axis are 0.52, 0.82, 1.12, and 1.42 m, respectively. This is the main accomplishment of the developed procedure. The variation of the anisotropy parameter T produced differences in the results, with a tendency of moving the separation point upstream when T was decreased from unity. The calculation with $T=1$ predicted the separation closer to its measured location. The upwinding parameter r used in these calculations is $r=0.12$. In the results shown the darkened symbols denote the experiments and the results shown are for $T=1$.

In conclusion, the inverse mode is used to compute turbulent boundary layers under the infinite swept cylinder assumption. The scheme reproduces with reasonable accuracy the trends in measured data, including the region of three-dimensional separation.

Acknowledgments

This work was supported by a grant from the Advanced Research Organization of the Lockheed-Georgia Company.

References

[1] Cousteix, J. and Houdeville, R., "Singularities in Three-Dimensional Turbulent Boundary-Layer Calculations and Separation Phenomena," *AIAA Journal*, Vol. 19, Aug. 1981, pp. 976-985.

[2] Catherall, D. and Mangler, K. W., "The Integration of Two-Dimensional Laminar Boundary Layer Equations Past the Point of Vanishing Skin Friction," *Journal of Fluid Mechanics*, Vol. 26, Pt. 1, 1966, pp. 163-182.

[3] Klineberg, J. M. and Steger, J. L., "On Laminar Boundary-Layer Separation," AIAA Paper 74-94, 1974.

[4] Carter, J. E., "Inverse Boundary-Layer Theory and Comparison with Experiment," NASA TP-1208, 1978.

[5] Carter, J. E. and Wornom, S. F., "Forward Marching Procedure for Separated Boundary-Layer Flows," *AIAA Journal*, Vol. 13, Aug. 1975, pp. 1101-1103.

[6] Cebeci, T., "An Inverse Boundary-Layer Method for Compressible Laminar and Turbulent Boundary Layers," *Journal of Aircraft*, Vol. 13, Sept. 1976, pp. 709-717.

[7] Cebeci, T., Keller, H. B., and Williams, P. G., "Separating Boundary-Layer Flow Calculations," *Journal of Computational Physics*, Vol. 31, June 1979, pp. 363-378.

[8] Pletcher, R. H., "Prediction of Incompressible Turbulent Separating Flow," *Journal of Fluid Engineering*, Vol. 100, Dec. 1978, pp. 427-433.

[9] Horton, H. P., "Comparisons Between Inverse Boundary-Layer Calculations and Detailed Measurements in Laminar Separated Flows," *The Aeronautical Quarterly*, Vol. XXXII, Pt. 3, Aug. 1981, pp. 169-187.

[10] Carter, J. E., "Viscous-Inviscid Interaction Analyses of Transonic Turbulent Separated Flow," AIAA Paper 81-1241, 1981.

[11] Gordon, R. and Rom, J., "Transonic Viscous-Inviscid Interaction Over Airfoils for Separated Laminar on Turbulent Flows," *AIAA Journal*, Vol. 19, May 1981, pp. 545-552.

[12] Wigton, L. B. and Holt, M., "Viscous-Inviscid Interaction in Transonic Flow," AIAA Paper 81-1003, 1981.

[13] Vatsa, V. N., Werle, M. J., and Verdon, J. M., "Viscid/Inviscid Interaction at Laminar and Turbulent Symmetric Trailing Edges," AIAA Paper 82-0165, 1982.

[14] Whitfield, D. L., Swafford, T. W., and Jacobs, J. L., "Calculation of Turbulent Boundary Layers with Separation and Viscous/Inviscid Interaction," *AIAA Journal*, Vol. 19, Oct. 1981, pp. 1315-1322.

[15] Carter, J., "A New Boundary-Layer Inviscid Interaction Technique for Separated Flow," AIAA Paper 79-1450, 1979.

[16] *Flow Separation, AGARD Conference Proceedings*, No. 168, 1975.

[17] Ragab, S., "Interacting Laminar Viscous Flows and Some Aspects of Their Stability," Ph.D. Dissertation, Virginia Tech., Blacksburg, Va., 1979.

[18] Johnson, D. A., Hortsman, C. C., and Bachalo, W. D., "Comparison Between Experiment and Prediction for Transonic Turbulent Separated Flow," *AIAA Journal*, Vol. 20, June 1982, pp. 737-744.

[19] Simpson, R. L., Chew, Y. T., and Shiraprassad, B. G., "The Structure of a Separating Turbulent Boundary Layer," *Journal of Fluid Mechanics*, Parts 1, 2, and 3, Vol. 113, 1981, pp. 23-91.

[20] Ramaprian, B. R., Patel, V. C., and Choi, D. H., "Mean Flow Measurements in the Three-Dimensional Boundary Layer Over a Body of Revolution at Incidence," *Journal of Fluid Mechanics*, Vol. 103, Feb. 1981, pp. 479-504.

[21] Rotta, J. C., "A Family of Turbulence Models for Three-Dimensional Boundary Layers," *Proceedings of 1st Symposium on Turbulent Shear Flows*, Vol. I, 1977.

[22] Bradshaw, P., Cebeci, T., and Whitelaw, J., *Engineering Calculation Methods for Turbulent Flow*, Academic Press, New York, 1981.

[23] Van den Berg, B., Elsenar, A., Lindhout, J.P.F., and Wesseling, P., "Measurements in an Incompressible Three-Dimensional Turbulent Boundary Layer Under Infinite Swept Wing Conditions and Comparison with Theory," *Journal of Fluid Mechanics*, Vol. 70, Jan. 1975, p. 127.

[24] *Turbulent Boundary Layers: Experiments, Theory and Modeling, AGARD Conference Proceedings*, No. 271, 1980.

[25] Formery, M. and Delery, J., "Methode aux differnce finies pur le calcul en mode inverse de la couche limite turbulente tridimensionnell," *La Recherche Aerospaciale*, Annee, No. 5, Sept.-Oct. 1981, pp. 303-313.

[26] Delery, J. M. and Formery, M. J., "A Finite Difference Method for Inverse Solutions of 3-D Turbulent Boundary-Layer Flow," AIAA Paper 83-0301, 1983.

[27] Delery, J. M. and Veuillot, J. P., "Recherches Experimentales et Theoretique sur la Turbulence dans les Interactions Choc-Couche Limite en Transonique," ONERA TP 1982-77, 1982.